Direct Observation of Resonance Motion in Complex Elimination Reactions: Femtosecond Coherent Dynamics in Reduced Space

ARTICLE *in* THE JOURNAL OF PHYSICAL CHEMISTRY A · MARCH 2001

Impact Factor: 2.69 · DOI: 10.1021/jp0041499

4 AUTHORS, INCLUDING:

Eric Diau
National Chiao Tung University
140 PUBLICATIONS **7,960** CITATIONS

SEE PROFILE

THE JOURNAL OF PHYSICAL CHEMISTRY A

 VOLUME 105, NUMBER 10, MARCH 15, 2001

LETTERS

Direct Observation of Resonance Motion in Complex Elimination Reactions: Femtosecond Coherent Dynamics in Reduced Space

Carsten Kötting, Eric W.-G. Diau, John E. Baldwin,† and Ahmed H. Zewail*

Arthur Amos Noyes Laboratory of Chemical Physics, California Institute of Technology, Pasadena, California 91125

Received: November 9, 2000; In Final Form: January 24, 2001

In this communication we report the observation of a resonant, coherent nuclear motion in the elimination reaction of 1,3-dibromopropane (DBP), a system with 27 internal degrees of freedom. The system was investigated using femtosecond time-resolved mass spectrometry, following excitation at a total energy $E =$ 186 kcal mol^{-1} ($n \rightarrow$5p Rydberg state). The vibrational coherence was observed with a period of 680 fs corresponding to the torsional vibration involving the two C−Br bonds. The C−Br bond cleavage occurs with a reaction time of 2.5 ps and yields the 3-bromopropyl radical, which subsequently reacts (cleavage of the second C−Br bond and ring closure) to give cyclopropane in 7.5 ps. These results elucidate the elementary steps and the mechanism: In a reduced space of two coordinates, the reaction coordinate involves a coherent torsional motion and C−Br bond rupture. Density functional theory (DFT) and time-dependent DFT calculations were carried out to detail the potential energy surface.

I. Introduction

The preparation of a wave packet on the global potential energy surface (PES) is the key for observing coherent trajectories of reactions.[1] When the superposition includes many vibrational eigenstates on the femtosecond (fs) time scale, the packet moves similar to a classical particle, defining the period and the frequency of the vibrational nuclear motion. To observe such coherence of motion, a probe "window" at a given configuration and an initial localization of the packet are two conditions that must be satisfied. For reactive simple systems, the prototype example for such a behavior is sodium iodide (NaI), where the observed coherent motion describes the resonance trajectory *along* the reaction coordinate.[2] For reactions involving polyatomics, motion perpendicular to the reaction coordinate, including intramolecular vibrational energy redistribution (IVR), must be part of the description. However, because of the nature of femtosecond preparation, a reduced two(or a few)-dimensional picture defines the reactive pathway, which includes not only the bond-rupture coordinate but also the nonreactive mode(s) perpendicular to it, as shown in Figure 1. The first examples to elucidate such a behavior were those of the dissociation reaction of CH_3I[3,4] and the isomerization of *cis*-stilbene in the gas phase[5] and in solution.[6] Examples have been reported for reactions involving multiple steps ($Cr(CO)_6$),[7] proton transfer in solution,[8] *trans*−*cis* isomerization,[9] and biological systems (see, e.g., refs 10−12).

Here, we report real-time observation of vibrational coherence in 1,3-dibromopropane (DBP) using femtosecond time-resolved mass spectrometry in a molecular beam. This system is unique in that there is only σ-type bonding and the vibrational motions are distinct. We investigated the wave packet motion on the PES of the $n \rightarrow$5p Rydberg state. The observed modulated signal has a period of 680 fs, which corresponds to a torsional motion with the vibrational frequency of 49 cm^{-1}. The dephasing of

† Permanent address: Department of Chemistry, Syracuse University, Syracuse, NY 13244-4100.

10.1021/jp0041499 CCC: $20.00
Published on Web 02/20/2001

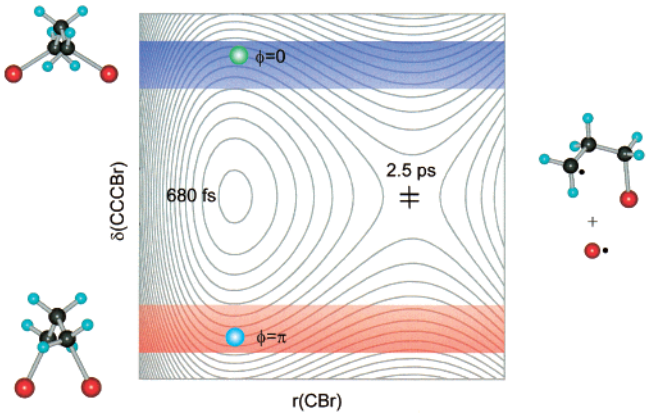

Figure 1. Reduced two-dimensional picture representing the dynamics of the polyatomic system studied here. The nonreactive coordinate corresponds to the torsional vibration and the reactive coordinate corresponds to the C−Br bond-breaking process with a barrier shown as ‡. The two positions shown for the packet (green, blue) represent the motion along the nonreactive coordinate for several periods, between the $\delta = 60°$ and $\delta = 30°$ structures, and the subsequent C−Br bond cleavage. Note that the localized femtosecond preparation is essential for the observation of coherence and nonstatistical behavior; the two windows of observation are shown for the phase $\phi = 0$ (blue), π (red). The initial wave packet, not shown, begins the motion from the repulsive wall.

coherence and the overall decay of the signal describe the process of C−Br bond breakage, which leads to the intermediate (3-bromopropyl radical) with a time constant of 2.5 ps. Furthermore, the 3-bromopropyl radical intermediate undergoes ring closure and C−Br bond cleavage with a time constant of 7.5 ps; this channel has the lowest barrier, 17 kcal mol^{-1}. Density functional theory (DFT) and time-dependent (TD) DFT calculations have been performed for the ground-state, excited-state, and cationic ground-state PES's, and the results support our reduced two-dimensional model for the dynamics: The reaction trajectory involves vibrational coherence along the symmetrical δ(CCCBr) torsion with motion along the C−Br reactive coordinate (Figure 1).

II. Experimental and Theoretical Methods

The experimental setup consisted of a femtosecond laser system (615 nm, ∼150 μJ pulse^{-1}, ∼80 fs) in combination with a molecular beam system.[13] The femtosecond pulse was split into two parts to provide pump and probe beams. For the pump, the 615-nm output was frequency-doubled. The time delay was controlled by a translation stage, which alters the path length of the probe pulse. The two beams were spatially combined and focused onto the supersonic molecular beam. Pump and probe beams were appropriately attenuated to optimize the enhancement of the ionization when both pump and probe pulses were present. The polarization angle of the probe beam relative to that of the pump beam was fixed at 54.7° (magic angle). The resulting ions were detected by a time-of-flight (TOF) mass spectrometer.

DBP (99%, Aldrich) was used without further purification; the mass spectrum is consistent with reported peaks.[14] 2,2-d_2-DBP was synthesized by a procedure described in the literature.[15] According to reported electron diffraction studies, the most stable conformation of DBP has the *gauche*−*gauche* structure (Figure 2A).[16]

Calculations were performed using the Gaussian 98 program package.[17] Geometries and energies were calculated at the B3LYP/6-31+G(d) level of theory. All energies of ground-state species include the zero-point energy (ZPE). Excited states were

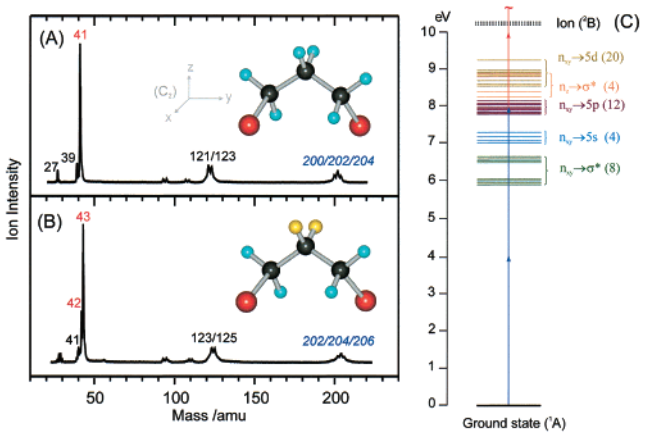

Figure 2. Femtosecond time-resolved mass spectra of (A) DBP and (B) 2,2-d_2-DBP obtained at a delay time of ∼50 fs. (C) Excitation/ionization scheme for the observed transient signals. All transition energies were obtained using TDDFT calculations at the B3P86/6-311++G(d,p) level, neglecting spin−orbit coupling. In parentheses we give the number for each type of the transitions involved.

calculated at the TD-B3LYP/6-31+G(d) or the TD-B3P86/6-311++G(d,p) level of theory using the optimized geometry of the ground state. Details of such calculations will be given in a full report.

III. Results and Data Analyses

The multiphoton ionization (MPI) mass spectra of DBP and 2,2-d_2-DBP are shown in Figure 2A,B, respectively. There are two major features displayed in both mass spectra. First, the ion signals at the parent mass $M^{\bullet+}$ and the fragment mass $[M - Br]^+$ are characterized by a triplet and a doublet mass pattern, which are due to the nearly equal abundance of the two Br isotopes. Second, the most prominent ion signal is located at 41 amu for DBP and at 43 amu for 2,2-d_2-DBP. Note that there is also substantial abundance (∼40%) for the 42 amu ion signal shown in the mass spectrum of 2,2-d_2-DBP. The appearance of 121/123 amu (123/125 amu for 2,2-d_2-DBP) indicates that the first step in ion fragmentation is the loss of Br (not HBr/DBr). The subsequent elimination of HBr from the 121/123 amu (HBr/DBr from the 123/125 amu for 2,2-d_2-DBP) ion species gives rise to the 41 amu (43/42 amu for 2,2-d_2-DBP) signal. Thus this observation indicates that the ion signal of the 41 amu in DBP (or 42 and 43 amu in 2,2-d_2-DBP) actually results from the $[M - Br]^+$.[18] As discussed below, this result is entirely consistent with the fact that both 42/43 amu give the same femtosecond transients.

Figure 3 shows the ion signal as a function of the delay time for the 202 and 41 amu masses of DBP. The transient of the parent 202 amu has three components: (1) a femtosecond response near time zero, with a time constant τ_0; (2) a coherent modulation of the signal with a period τ_c, together with an overall decay (and dephasing) with a time constant τ_1; (3) a negative signal offset.[19] The complementary behavior of the transient for the 41 amu was analyzed similarly: (1) a femtosecond component as in the transient of 202 amu; (2) a coherent modulation of the signal with the same period as that of 202 amu (τ_c) *but with the phase shifted by exactly one-half a period* (π); (3) a buildup and dephasing (time constant τ_1) but with additional decay (time constant τ_2) which is absent in the transient of 202 amu; (4) a corresponding offset to that observed for the 202 transient but now positive. Note that the observed transients are due to reaction of the neutral species and not the ions. This is because probe ionization of the neutral

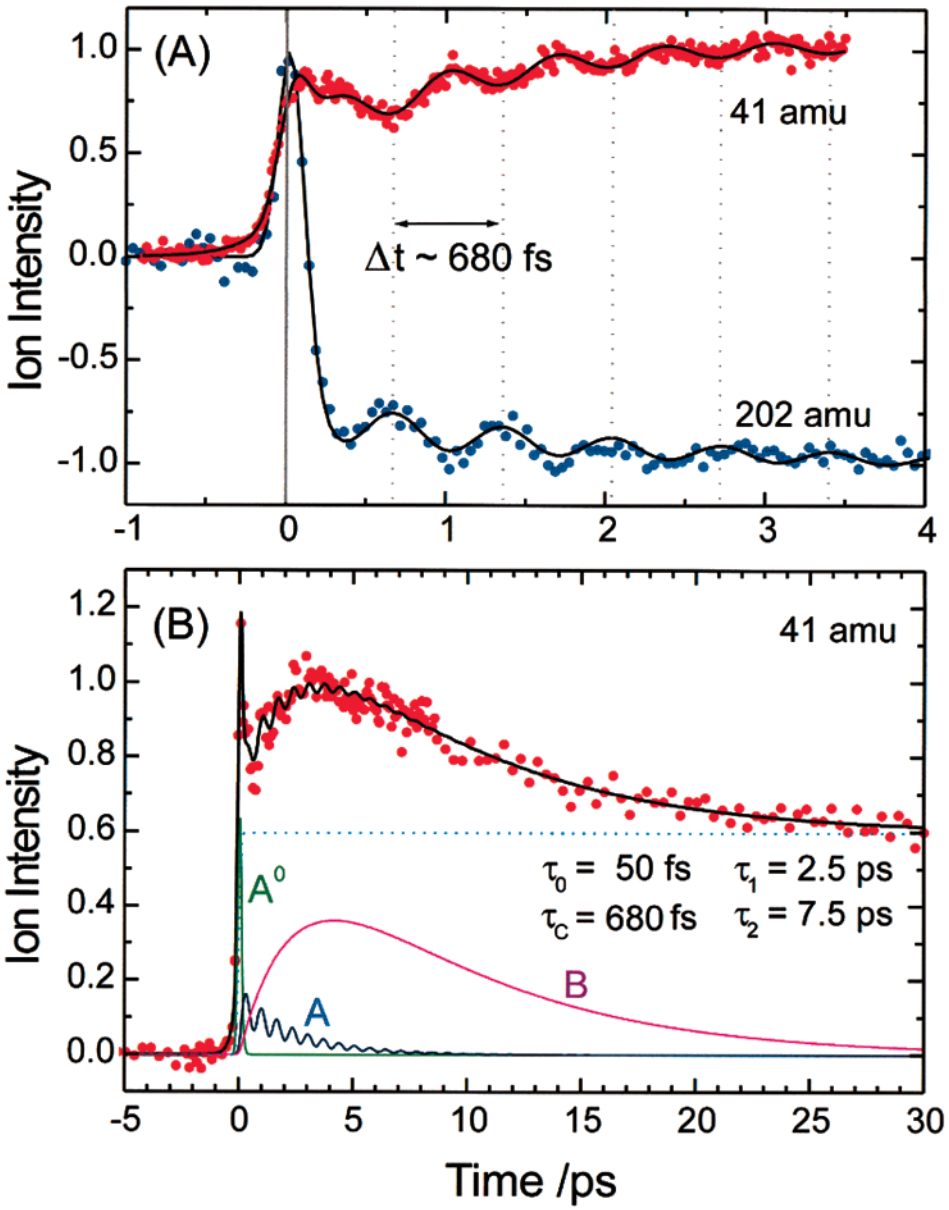

Figure 3. (A) Femtosecond transients of DBP for both the parent (202 amu) and the fragment (41 amu) mass, showing the modulated component with a constant period of 680 fs and the phase shift of exactly one-half a period between the two transients. Theoretical curves are also shown. (B) Transient of DBP (up to 30 ps) for the 41 amu, together with the theoretical fit indicating the change of population of A^0, A, and B according to the dynamical model detailed in the text. The dotted line is the offset described in the model (see text).

species gives enhancement of ion signal, while probe of an ion results in a depletion.[19] Furthermore, our observed femtosecond to picosecond time scale dynamics will not be observed on a parent ion since the time scale of mass spectroscopic detection is microseconds. Finally the transients of 121/123 amu show the same features as the transient of the parent mass, indicating that they result from fragmentation of the parent ion.

Accordingly, the same elementary steps are involved in the consecutive dynamical model for both 202 and 41 amu masses:

$$A^0 \xrightarrow{\tau_0} A \xrightarrow{\tau_1} B \xrightarrow{\tau_2} C \qquad (1)$$

Here, A^0 represents the initial ($t = 0$) Franck−Condon (FC) structure responsible for the femtosecond motion near time zero; A stands for the parent species which undergoes the coherent resonance motion; B stands for the intermediate (3-bromopropyl radical), which only appears in the transient of 41 amu; and C represents the final product, which is dark to our probe. The population of a species in the above model can easily be solved[20] to include the femtosecond response function.[21] The overall transient signal for 202 amu can thus be expressed as: $S_{202} = \alpha^0_{202}A^0(t) + \alpha_{202}A(t)$, where $A^0(t)$ is the population of the initial FC species decaying with τ_0 and $A(t)$ is the population of A (build up by τ_0 and decay by τ_1); α^0_{202} and α_{202} are related to the ionization cross sections and the efficiency of ion fragmentation. These processes describe the total population of a given species.

To account for the observed coherent motion of the A molecule trajectories, the signal must include the probe window detection at a time t. As shown below, α_{202} depends on the torsional motion δ. The time dependence of this motion can be described by a cosine function with the phase ϕ as shown in Figure 1. Therefore, our signal from the A population must follow:

$$S_{202}(A) = \bar{\alpha}_{202}\{1 + c\cos(t/\tau_c + \phi)\}A(t) \qquad (2)$$

where c is a constant. Note that the average signal over all δ configurations gives only $\bar{\alpha}_{202}\,A(t)$ with no coherence. Similarly, we express the signal for the 41 amu, which now must include the population of the intermediate $B(t)$. Figure 3 gives the comparison between the experimental and theoretical results. Using a nonlinear least-squares procedure, the best fit of all experimental data gives the following results: $\tau_0 = 50$ fs; $\tau_1 = 2.5$ ps; $\tau_2 = 7.5$ ps; $c = 0.38$. The period obtained is $\tau_c = 680$ fs with the phase alternating between 0 (for 202 amu) and π (for 41 amu). Excellent fits were also obtained for the transients of both 42 and 43 amu of 2,2-d_2-DBP using exactly the same time constants and phase shift.

IV. Discussion

The above-described model appropriately reproduces the observed femtosecond transients (Figure 3) for both DBP and 2,2-d_2-DBP species. The following points can now be made: First, the initial femtosecond signal observed for both parent and fragment reflects a multidimensional dephasing process. The initially prepared wave packet moves out of the FC region within the observed 50 fs. Second, after this initial motion, the wave packet executes the torsional motion ($\tau_c = 680$ fs) in a reduced vibrational space, out of the total 27 degrees of freedom in DBP (Figure 1). This projection of coherence is unique to wave packet coherent preparation, as opposed to a microcanonical state preparation. Third, this coherence has also been shown in the fragment transient (41 amu in DBP) but with the phase shifted by exactly one-half a period. The observed phase shift indicates that there is a significant change in the effective ionization cross section along the nonreactive coordinate (δ), as shown below. Fourth, the decay of coherence of the parent occurs in 2.5 ps, reflecting the bond breakage in the C−Br coordinate, which is perpendicular to the δ motion. Finally, the intermediate (3-bromopropyl radical) is formed in 2.5 ps and decays in 7.5 ps. This channel is supported by our DFT calculations given below.

A. Coherence Along the Torsional Coordinate δ(CCCBr). The ground-state DBP has only one vibration with a low frequency (~50 cm^{-1}),[16,22] having a period similar to the time scale of the observed coherence ($\tau_c = 680$ fs). It is the symmetrical δ(CCCBr) torsion with **A** symmetry (C_2). According to our TDDFT calculations of the vertical excitation spectrum of DBP, the absorption of two pump photons brings the molecule into a $n_{xy}\rightarrow$5p Rydberg state (Figure 2C). Generally, the vibrational modes of a Rydberg state are similar to those of the ground state. Therefore, the observed vibrational coherence suggests that it is the torsional motion that has been activated upon excitation.

We have carried out DFT/TDDFT calculations with the results shown in Figure 4: a dramatic change of energy along the torsional coordinate. This change is due to the strong through-space and through-bond interactions when two Br atoms follow this torsional motion to approach close to each other. Figure 4A shows the energy change along the δ coordinate for the four highest occupied nonbonding orbitals (n_{xy}). The weaker π-type interaction for the n_x-type orbitals gives a smaller splitting between the n_xA and n_xB orbitals, but the somewhat stronger σ-type interaction for the n_y-type orbitals leads to a larger separation between the n_yA and n_yB orbitals.

The calculated PES reflects this orbital description.[23] For the neutral ground state, the energy increases from the minimum ($\delta = 60°$) along the torsional coordinate toward smaller angles, since all n_{xy} orbitals are doubly occupied. On the other hand, the opposite energy change of the cation is apparently due to

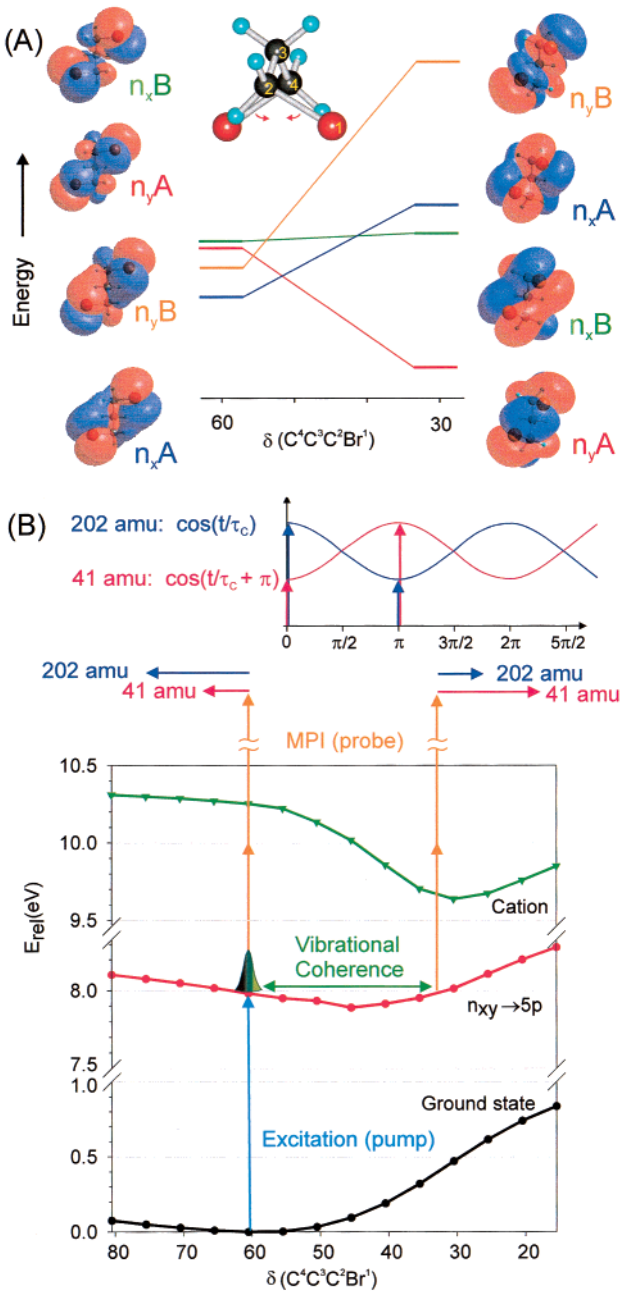

Figure 4. (A) DFT results showing the orbital correlation diagram of DBP. The four highest occupied Kohn−Sham orbitals were obtained along the δ(CCCBr) torsional coordinate at the B3LYP/6-31+G(d) level of theory. These nonbonding n_x and n_y lone pair orbitals involving the two Br atoms are shown, less interactive at $\delta = 60°$ and strongly interacting at $\delta = 30°$. In the ground state, these orbitals are occupied (8 electrons), but as δ decreases from 60° to 30°, the antibonding order increases, hence the increase in the ground state potential energy. On the other hand, in the cation, the highest occupied orbital is only singly occupied, resulting overall in higher bonding order and hence the decrease in potential energy. (B) Potential energy change along the δ coordinate for the ground state, Rydberg, and the cation. Note the dramatic change as the molecule twists from 60° to 30° (structures shown in Figure 1). Although the minimum is somewhat shifted for the Rydberg from the ground state, the curvatures are similar.

the fact that the HOMO is only singly occupied. As a result the minimum energy of the cation is calculated to be at $\delta = 30°$ with the two Br atoms separated by only 2.89 Å (equilibrium distance of $Br_2 = 2.28$ Å).

Promotion of an electron from either of the four nonbonding orbitals into one of the three different 5p Rydberg orbitals gives

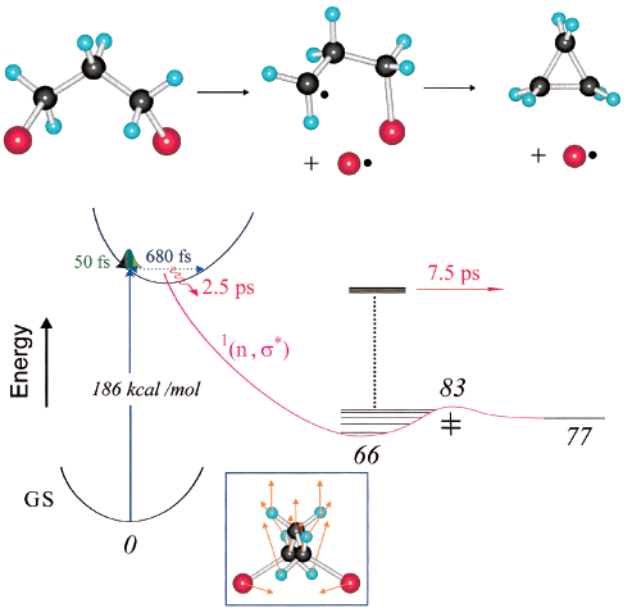

Figure 5. Molecular structures and reaction coordinate (RC) describing the observed dynamics of the reaction. Shown are the time scales involved and the values for the energies (relative to the ground state) in kcal mol^{-1}, calculated at the B3LYP/6-311G(d,p)//6-31G(d,p) level of theory with ZPE corrections. The inset shows the calculated normal coordinate vectors for the ground-state torsional vibration.

rise to a total of 12 excitations corresponding to the $n_{xy}\rightarrow 5p_{xyz}$ Rydberg states (Figure 2C). The potential energy curves of these Rydberg states vary differently along δ, and the overall picture gets even more complicated if spin−orbit coupling is considered. However, the curve corresponding to the $n_xA\rightarrow 5p_x$ excitation (Figure 4B) is most likely the one responsible for the observed coherence for two reasons: First, the overall potential energy is very close to our excitation energy (8 eV). Second, the torsional frequency can be estimated using a harmonic oscillator model, which gives a value (∼45 cm^{-1}) very close to the value obtained from the observed coherent period (49 cm^{-1}). From the PES of Figure 4B, the origins of selectivity and phase shift are understood.

B. Nonconcerted Elimination Reaction. The first elementary step occurs with $\tau_1 = 2.5$ ps to yield the intermediate B. To identify B as 3-bromopropyl radical, i.e., Br-elimination (not HBr-elimination), we have investigated the dynamics of 2,2-d_2-DBP. As discussed above for the ions, neutral $\cdot CH_2CD_2CH_2Br$ upon ionization gives the corresponding ion, which produces the 42/43 amu. Thus the observation of the same dynamical behavior for both species indicates their formation from 3-bromopropyl radical as the intermediate (B). Furthermore, the lack of a kinetic isotope effect for τ_1 is also against the HBr(DBr)-elimination mechanism. Thus, all our experimental evidence supports that it is the C−Br bond-breaking process that gives the 3-bromopropyl radical as the intermediate B described in eq 1.

The theoretical calculations are consistent with the above picture. Our TDDFT surface scan calculations demonstrate that the $n_xA\rightarrow 5p_x$ Rydberg surface strongly interacts with the repulsive $n_z\rightarrow\sigma^*$ surfaces along the C−Br bond-breaking coordinate. As a result, the overall C−Br bond-breaking process can be described by a diabatic surface with a small barrier all the way down to the ground-state PES. Our calculations also show many curve crossings between the $n_xA\rightarrow 5p_x$ Rydberg and the other (n,5p) Rydberg surfaces along the δ coordinate. Therefore, it is also possible for the C−Br bond-breaking process to occur through the lower repulsive $n_{xy}\rightarrow\sigma^*$ surfaces, which may be reached by Landau−Zener crossings of excited-state surfaces. The observed 2.5-ps decay may be due to either the barrier crossing process of the diabatic case or the Landau−Zener curve crossings in a nonadiabatic model.

As for the second step of the reaction, both the isotope-substitution experiments and the theoretical calculations support the following picture: The intermediate 3-bromopropyl radical (B) undergoes a "concerted" Br-elimination and ring-closure reaction to yield cyclopropane and Br atom as final products. This conclusion is based on the fact that the Br-elimination to yield trimethylene requires 65.6 kcal mol^{-1}, whereas the concerted reaction has a barrier of only 17 kcal mol^{-1} (B3LYP/6-311G(d,p)//6-31G(d,p) + ZPE). Because the lifetime of the 3-bromopropyl radical was observed to be 7.5 ps for both DBP and 2,2-d_2-DBP species, reactions involving H(D)-migration, H(D)-elimination, or H(D)Br-elimination are less likely. Furthermore, we have calculated the energy barriers for these reaction channels and found them to be in energy: 32, 36, and 40 kcal mol^{-1}, respectively. Our transition state for the latter is consistent with that calculated for the reverse reaction.[24]

V. Conclusion

In summary, the polyatomic elimination reaction reported here (Figure 5) exhibits coherent and selective dynamics. The following describes the elementary steps involved. (1) An initial wave packet is prepared on the global PES. (2) The wave packet moves away from the FC region within the observed 50 fs. (3) The observed coherent motion with a period of 680 fs is along the δ(CCCBr) torsional coordinate. (4) The dephasing of coherence and the overall reaction in 2.5 ps takes place along the C−Br bond-breaking coordinate to yield the 3-bromopropyl radical intermediate. (5) The subsequent reaction in 7.5 ps is the result of a "concerted" Br-elimination and ring-closure process with an energy barrier of 17 kcal mol^{-1} on the ground-state PES. These findings are supported by DFT and TDDFT calculations. The reduced dimensionality picture and the experimental observation of coherent trajectories in polyatomic systems are the consequences of femtosecond coherent preparation (and window probing) and will be suppressed (mimicking a statistical behavior) if microcanonical state preparation is involved.[25,26]

Acknowledgment. This work was supported by the U.S. Air Force Office of Scientific Research and the Office of Naval Research. C.K., a Feodor Lynen Fellow from the Alexander von Humboldt Foundation, acknowledges the foundation and Caltech for support. We thank Dharmesh B. Patel and Dr. Rajesh Shukla of Syracuse University for the preparation of the deuterium-labeled DBP. We are grateful to the summer research fellows Wee Kang Chua and Frank Ducheneaux for their assistance and to Dr. Klaus Møller and Profs. John D. Roberts and Joseph Casanova for helpful discussions.

References and Notes

(1) Zewail, A. H. *J. Phys. Chem. A* **2000**, *104*, 5660−5694 and references therein.
(2) Mokhtari, A.; Cong, P.; Herek, J. L.; Zewail, A. H. *Nature* **1990**, *348*, 225−227.
(3) Janssen, M. H. M.; Dantus, M.; Guo, H.; Zewail, A. H. *Chem. Phys. Lett.* **1993**, *214*, 281−289.
(4) Guo, H.; Zewail, A. H. *Can. J. Chem.* **1994**, *72*, 947−957.
(5) Pedersen, S.; Bañares, L.; Zewail, A. H. *J. Chem. Phys.* **1992**, *97*, 8801−8804.
(6) Szarka, A. Z.; Pugliano, N.; Palit, D. K.; Hochstrasser, R. M. *Chem. Phys. Lett.* **1995**, *240*, 25−30.
(7) Trushin, S. A.; Fuss, W.; Schmid, W. E.; Kompa, K. L. *J. Phys. Chem. A* **1998**, *102*, 4129−4137.

(8) Lochbrunner, S.; Wurzer, A. J.; Riedle, E. *J. Chem. Phys.* **2000**, *112*, 10699−10702.

(9) Takeuchi, S.; Tahara, T. *Chem. Phys. Lett.* **2000**, *326*, 430−438.

(10) Sundström, V. *Femtochemistry and Femtobiology: Ultrafast Reaction Dynamics at Atomic-Scale Resolution*; Imperial College Press. World Scientific Publishing Co. Pte. Ltd.: Singapore, 1996.

(11) Gonzalez-Luque, R.; Garavelli, M.; Bernardi, F.; Merchan, M.; Robb, M. A.; Olivucci, M. *Proc. Natl. Acad. Sci. U.S.A.* **2000**, *97*, 9379−9384.

(12) Eaton, W. A. *Proc. Natl. Acad. Sci. U.S.A.* **1999**, *96*, 5897−5899.

(13) Zewail, A. H. *Femtochemistry: Ultrafast Dynamics of the Chemical Bond*; World Scientific: Singapore, 1994; Vol. I and II and references therein.

(14) Mallard, W. G.; Linstrom, P. J. *NIST Chemistry WebBook, NIST Standard Reference Database Number 69*; National Institute of Standards and Technology: Gaithersburg, MD, 2000.

(15) Baldwin, J. E.; Patel, D. B. *J. Labeled Compd. Radiopharm.* **1999**, *42*, 55−61.

(16) Farup, P. E.; Stølevik, R. *Acta Chem. Scand. A* **1974**, *28*, 680−692.

(17) Frisch, M. J.; et al. *Gaussian*, revision A.9; Gaussian, Inc.: Pittsburgh, PA, 1998.

(18) Danon, A.; Amirav, A. *J. Phys. Chem.* **1989**, *93*, 5549−5562.

(19) Under our experimental conditions, some DBP is ionized by the pump pulse alone through the absorption of at least three photons, and this gives a background signal for the parent and fragment masses at negative delay times. At positive delay times, the background ion signal at 202 amu is constantly decreased while that at 41 amu is constantly increased, due to parent ion fragmentation by the probe pulse. This explains why we always obtain a negative signal offset in the parent transient (202 amu) and a positive offset in the fragment transient (41 amu). We had to maintain a relatively strong pump energy in order to clearly see the modulation with large S/N.

(20) Steinfeld, J. I.; Francisco, J. S.; Hase, W. L. *Chemical Kinetics And Dynamics*, 2nd ed.; Prentice Hall: Upper Saddle River, NJ, 1999.

(21) Pedersen, S.; Zewail, A. H. *Mol. Phys.* **1996**, *89*, 1455−1502.

(22) Gustavsen, J. E.; Klaeboe, P.; Stølevik, R. *J. Mol. Struct.* **1978**, *50*, 285−291.

(23) The calculated values for the energy of the cation are scaled by a factor of 0.96 (4% correction) in order to match the experimental vertical ionization potential.[14]

(24) Coxon, J. M.; Smith, W. B. *J. Org. Chem.* **2000**, *65*, 2192−2194.

(25) Diau, E. W.-G.; Herek, J.; Kim, Z. H.; Zewail, A. H. *Science* **1998**, *279*, 847−851.

(26) Møller, K. B.; Zewail, A. H. *Helv. Chim. Acta* **2000**, to be published.